NJC

Accepted Manuscript

This is an *Accepted Manuscript*, which has been through the Royal Society of Chemistry peer review process and has been accepted for publication.

Accepted Manuscripts are published online shortly after acceptance, before technical editing, formatting and proof reading. Using this free service, authors can make their results available to the community, in citable form, before we publish the edited article. We will replace this *Accepted Manuscript* with the edited and formatted *Advance Article* as soon as it is available.

You can find more information about *Accepted Manuscripts* in the Information for Authors.

Please note that technical editing may introduce minor changes to the text and/or graphics, which may alter content. The journal's standard Terms & Conditions and the Ethical guidelines still apply. In no event shall the Royal Society of Chemistry be held responsible for any errors or omissions in this *Accepted Manuscript* or any consequences arising from the use of any information it contains.

ROYAL SOCIETY OF CHEMISTRY

www.rsc.org/njc

NJC

RSCPublishing

LETTER

Cyano-Bridged Coordination Polymer Gel as a Precursor to Nanoporous In_2O_3–Co_3O_4 Hybrid Network for High-Capacity and Cycle-Stable Lithium Storage

Cite this: DOI: 10.1039/c3nj00000x

Received 00th XXXXX 2013,
Accepted 00th XXXXX 2013

DOI: 10.1039/c3nj00000x

www.rsc.org/njc

Weiyu Zhang,[§] Jinjing Zhang,[§] Meiling Zhang, Chenxing Zhang, Anping Zhang, Yiming Zhou, Yawen Tang and Ping Wu*

A novel type of nanoporous In_2O_3–Co_3O_4 hybrid network has been synthesized using a cyano-bridged coordination polymer gel as a precursor. When applied as an anode in lithium-ion batteries, the In_2O_3–Co_3O_4 network manifests remarkable capacity retention and high reversible capacities by virtue of its unique compositional and structural features.

As important categories of anodic materials in lithium-ion batteries (LIBs), metal oxides have been considered to be ideal anodic candidates to replace commercial graphite-based materials owing to their higher safety and specific capacities.[1-15] Among them, indium oxide (In_2O_3) possesses similar alloying/de-alloying lithium-storage mechanism to other main-group metal oxides including SnO_2,[7-9] GeO_2,[10,11] and so forth. Generally, the lithium-storage processes of In_2O_3 can be described as follows: $In_2O_3 + 6Li^+ + 6e^- \rightarrow 2In + 3Li_2O$ (eqn 1); $In + 4.33Li^+ + 4.33e^- \leftrightarrow Li_{4.33}In$ (eqn 2).[12-15] Despite the improved safety and higher theoretical capacities, the formation of inactive Li_2O (eqn 1) gives rise to large Li^+-consumption and initial capacity loss, meanwhile the alloying/de-alloying processes described by eqn 2 lead to huge volume variations, progressive pulverization, and fast capacity decay.

Recently, it has proved that nanostructuring and hybridizing SnO_2 anodes with transition-metal oxides (M_xO_y, M = Mn,[16] Fe,[17-20] Co,[21] Ni,[22-24] Cu,[25] Mo,[26] W,[27] etc) could serve as an effective solution to reduce the initial irreversible capacity and improve the cycling stability of SnO_2-based anodes. The *in situ* generated transition-metal nanocrystals from M_xO_y can activate/promote the decomposition of Li_2O and reversible formation of polymeric gel-like layer and thus increase their Coulombic efficiencies and reversible capacities, meanwhile the stepwise Li-storage reactions at different potentials of SnO_2 and M_xO_y together with rationally designed nanostructure can effectively accommodate the volume changes and improve the cycling performance of the SnO_2–M_xO_y nanohybrids.[16-27] Therefore, In_2O_3–M_xO_y nanohybrids are anticipated to exhibit similar performance-enhancement mechanisms and manifest ideal lithium-storage performances for advanced LIBs.[15-27]

As inspired by this, we have rationally designed and synthesized a novel type of In_2O_3–M_xO_y nanohybrids, i.e., nanoporous In_2O_3–Co_3O_4 hybrid network, *via* a facile freeze-drying and subsequent annealing approach using a cyano-bridged In(III)–Co(III) bimetallic coordination polymer gel (i.e., $InCl_3$–$K_3Co(CN)_6$ cyanogel) as a precursor (Fig. 1). When utilized as an anode in LIBs, the as-prepared In_2O_3–Co_3O_4 network manifests excellent capacity retention and high reversible capacities by virtue of its unique compositional and structural features.

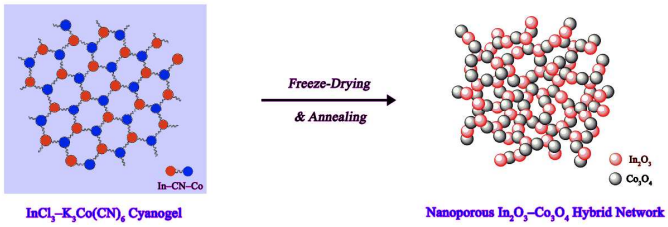

Fig. 1 Schematic diagram for the synthesis of the nanoporous In_2O_3–Co_3O_4 hybrid network.

Cyano-bridged coordination polymer gels (abbreviated as cyanogels) are formed *via* the reaction of solutions of chlorometalates (K_2PtCl_4,[28] K_2PdCl_4,[29] $SnCl_4$,[24,30] etc) and transition-metal cyanometalates including $K_3Co(CN)_6$, $K_2Ni(CN)_4$, $K_4Fe(CN)_6$, and so forth, which experience sol-gel transitions to form stable gels. Cyanogels possess unique structural and compositional features in terms of three-dimensional (3D) porous framework and double-metallic property, and thus could serve as ideal precursors for porous alloy[28-30] and hybrid-oxide[24] networks with uniform distribution of metal species.

Herein, for the first time, a white-colored In(III)–Co(III)-based cyanogel (i.e., $InCl_3$–$K_3Co(CN)_6$ cyanogel) was conveniently obtained by simply mixing aqueous solutions of $InCl_3$ and $K_3Co(CN)_6$ at room temperature (Fig. 2). The molar ratio of In/Co in

the cyanogels can be easily adjusted by controlling the feeding ratios of $InCl_3$ and $K_3Co(CN)_6$ reactants, and this feature of $InCl_3$–$K_3Co(CN)_6$ cyanogels facilitates subsequent construction of alloy and hybrid-oxide products with controllable compositions and adjustable properties. As observed, stable $InCl_3$–$K_3Co(CN)_6$ cyanogels can be obtained at a series of feeding ratios of $InCl_3$ and $K_3Co(CN)_6$ from 2:1 (Fig. 2a), 1.5:1 (Fig. 2b), 1:1 (Fig. 2c), 1:1.5 (Fig. 2d), to 1:2 (Fig. 2e).

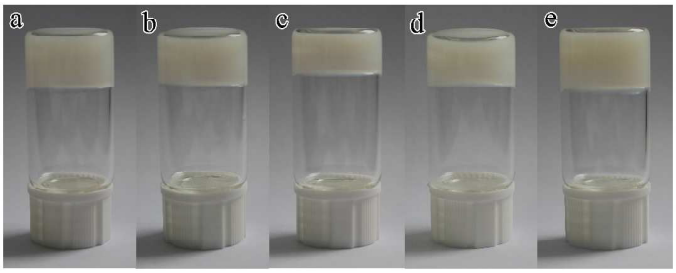

Fig. 2 Photographs of the $InCl_3$–$K_3Co(CN)_6$ cyanogels prepared by simply mixing aqueous solutions of 0.6 M $InCl_3$ and 0.6 M $K_3Co(CN)_6$ with different volume ratios: (a) 2:1, (b) 1.5:1, (c) 1:1, (d) 1:1.5, and (e) 1:2.

As a representative example, the physicochemical properties of the $InCl_3$–$K_3Co(CN)_6$ cyanogel with a In/Co molar ratio of 1:1 were examined by Fourier transform infrared (FTIR) spectra (Fig. 3). As observed, the FTIR spectrum of $K_3Co(CN)_6$ has a sharp cyano stretching vibration at 2130 cm^{-1} and a stretching vibration of ν(Co–C) at 565 cm^{-1} (curve *a*). According to the previous report, ν(C≡N) shifts to a higher frequency and ν(M–C) shifts to a lower frequency if the M–C≡N group forms a bridging cyano group of M–C≡N–M'.[31] Herein, the ν(C≡N) shifts to a higher frequency at 2199 cm^{-1}, meanwhile the ν(Co–C) shifts to a lower frequency at 465 cm^{-1} with a shoulder at 425 cm^{-1} in the freeze-dried $InCl_3$–$K_3Co(CN)_6$ cyanogel (curve *b*). This phenomenon can be attributed to the formation of bridging cyano groups of Co–C≡N–In by analogy to similarly bridged species including Co–C≡N–Pt[28] and Co–C≡N–Pd.[29] The FTIR results confirm the presence of bridging cyano groups (Co–C≡N–In) and thus the formation of cyano-bridged In(III)–Co(III) bimetallic coordination polymer gel.[28,29,31]

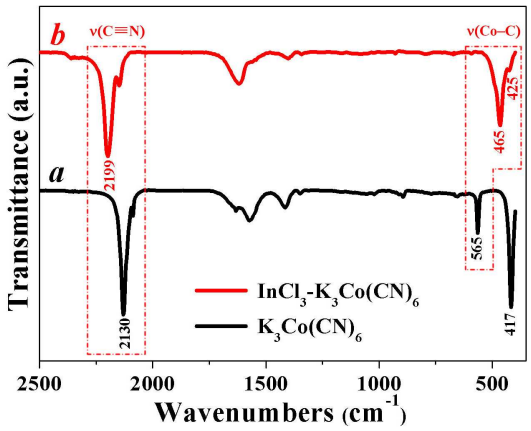

Fig. 3 FTIR spectra of the $K_3Co(CN)_6$ (curve *a*) and freeze-dried $InCl_3$–$K_3Co(CN)_6$ cyanogel (curve *b*).

The 3D porous structure feature and double-metallic composition characteristics of $InCl_3$–$K_3Co(CN)_6$ cyanogel make it an ideal precursor for the construction of porous In_2O_3–Co_3O_4 hybrid-oxide networks with uniform distribution and controllable ratios of In_2O_3 and Co_3O_4 components. As a proof-of-concept demonstration, nanoporous In_2O_3–Co_3O_4 hybrid network was facilely obtained through a freeze-drying and subsequent annealing route by using the $InCl_3$–$K_3Co(CN)_6$ cyanogel with a In/Co molar ratio of 1:1 as a precursor. The crystalline state of the prodcut was examined by X-ray powder diffraction (XRD) (Fig. 4). As observed, there are two set of diffraction peaks from the XRD pattern, which can be indexed to cubic In_2O_3 (JCPDS no. 65-3170) and cubic Co_3O_4 (JCPDS no. 43-1003), respectively. The XRD results indicate the successful formation of In_2O_3–Co_3O_4 hybrid oxides.

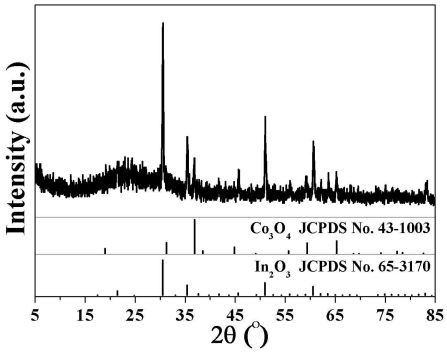

Fig. 4 XRD pattern of the nanoporous In_2O_3–Co_3O_4 hybrid network.

The morphological, compositional, and structural features of the In_2O_3–Co_3O_4 network has been examined by scanning electron microscopy (SEM) and transmission electron microscopy (TEM). As seen from SEM images, the product inherits the structural characteristics of the $InCl_3$–$K_3Co(CN)_6$ cyanogel precursor, and exists in the form of 3D porous network with particle size of about several microns to a dozen microns (Fig. S1). The TEM images further indicate that the In_2O_3–Co_3O_4 network is consisted of numerous nanocrystal building units and there are abundant nanopores within the network (Fig. 5a and c). Moreover, the high-resolution TEM (HRTEM) image clearly reveals the lattice fringes and interface region of two interconnected nanocrystals (Fig. 5d). As observed, the lattice fringe with lattice spacing of about 0.24 nm corresponds to the (311) plane of Co_3O_4 nanocrystals, and the two lattice fringes appeared at the adjacent nanocrystal with angle of 80.4° and spacing of 0.41 nm can be indexed to the (211) and (1-21) planes of In_2O_3 nanocrystals, respectively. The HRTEM results further confirm that the porous hybrid network is assembled by interconnected In_2O_3 and Co_3O_4 nanocrystals. Fig. 5b reveals the energy-dispersive X-ray spectrometer (EDS) spectrum of the In_2O_3–Co_3O_4 hybrid network. The observed strong peaks for In, Co, and O elements come from In_2O_3 and Co_3O_4 components, and the Cu elemental peak originate from the copper grid used in the TEM tests. Additionally, the molar ratio of indium and cobalt is determined to be 1.3:1 based on the EDS analysis, which is close to the feeding ratio of the $InCl_3$ and $K_3Co(CN)_6$ reactants. Moreover, the TEM-EDS elemental mapping reveals the uniform distribution of In, Co, and O elemental signals within the selected area and thus confirms the homogeneous distribution of In_2O_3 and Co_3O_4 nano-units in the hybrid network (Fig. 5e and f).

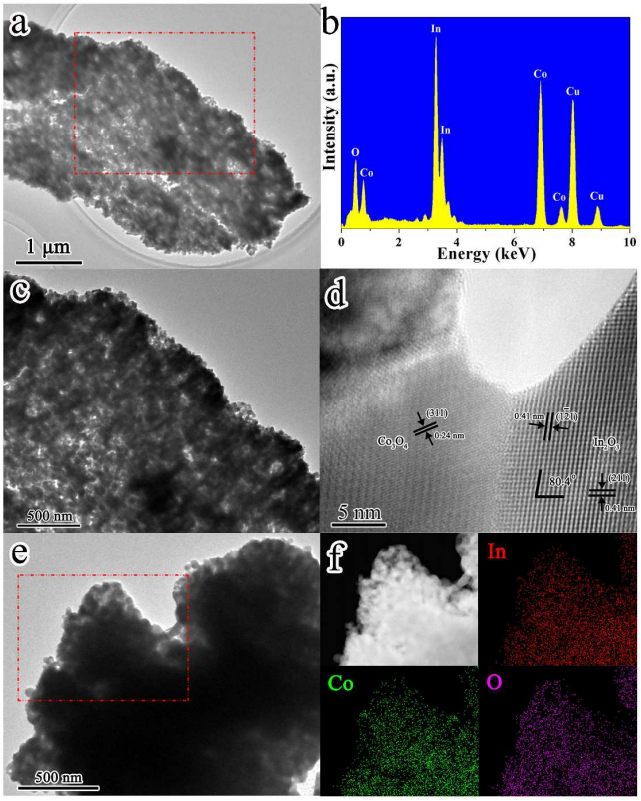

Fig. 5 Morphological, compositional, and structural features of the nanoporous In_2O_3–Co_3O_4 hybrid network: (a,c) TEM images, (b) EDS spectrum, (d) HRTEM image, and (e,f) TEM-EDS elemental mappings.

The surface area and pore volume of the hybrid network were further evaluated by nitrogen adsorption/desorption isotherms to demonstrate its porous characteristics (Fig. S2). As illustrated, the In_2O_3–Co_3O_4 network manifests a high Brunauer–Emmett–Teller (BET) surface area and a large Barrett–Joyner–Halenda (BJH) pore volume of 82.6 m^2 g^{-1} and 0.24 cm^3 g^{-1}, respectively. The high surface area and large pore volume of the In_2O_3–Co_3O_4 network is believed to benefit from the porous $InCl_3$–$K_3Co(CN)_6$ cyanogel precursor, and more importantly, is beneficial for the strain accommodation and electrolyte contact and thus the enhanced lithium-storage performance in terms of cycling stability and rate capability.[24,30]

Motivated by its unique compositional and structural features toward lithium-storage, the nanoporous In_2O_3–Co_3O_4 hybrid network was utilized as an anode material in LIBs. Fig. 6 reveals the cycling performance of the In_2O_3–Co_3O_4 network in the potential range of 0.01-3 V at a current density of 100 mA g^{-1}. As observed, the discharge capacities undergo a slowly fading process within the initial 20 cycles, which is mainly due to the formation of solid electrolyte interface (SEI) layer and locally slight pulverization within the network. Despite this, the In_2O_3–Co_3O_4 network manifests excellent capacity retention in subsequent cycles, and the reversible capacities keep steadily at about 630 mA h g^{-1} after 50 cycles. The *in situ* generated Co nanocrystals during lithium insertion in Co_3O_4 might act as an efficient catalyst to activate/promote the reversible formation of polymeric gel-like SEI layer[32,33] and also the oxidation of metallic indium and decomposition of Li_2O,[15-27,34] which can be largely responsible for the high capacity retention and reversible capacities. The voltage plateaus at about 2.5 V from the charge curves is more and more obvious upon cycling (Fig. 6a), which also suggests the probable existence of these catalytic processes by cobalt nanocrystals.[24,25] Thus, the In_2O_3–Co_3O_4 hybrid network is able to deliver a high reversible capacity of 638.7 mA h g^{-1} after 200 cycles, which is much higher than the theoretical capacity of graphite (372 mA h g^{-1}). The microscopic structural characterization after cycling confirms that the agglomeration and pulverization of hybrid oxide network can be effectively restrained during cycling (Fig. S3), and the enhanced structural stability of the hybrid network plays a key role in its improved Li-storage performance especially cycling stability. The high capacity retention and reversible capacities of the In_2O_3–Co_3O_4 network will pave the road for its practical utilization as a long-life and high-capacity anode material in advanced LIBs.

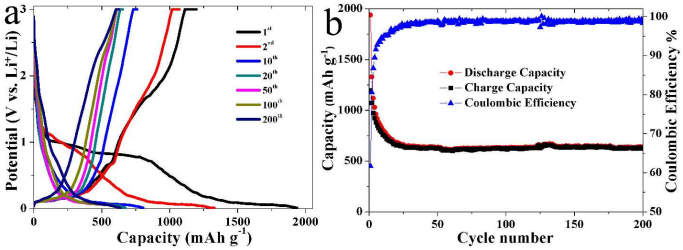

Fig. 6 Lithium storage performance of the nanoporous In_2O_3–Co_3O_4 hybrid network: (a) discharge and charge curves, and (b) cycling stability.

The excellent cycling performance and high reversible capacities of the In_2O_3–Co_3O_4 network can be attributed to its unique compositional and structural features. First, the 3D nanoporous network possesses the superiorities of both nano-building units and micro-assemblies toward lithium storage, and exhibits enhanced strain-accommodation and charge-transport capabilities during cycling.[24,30] Second, the stepwise Li-storage reactions at different potentials of In_2O_3 and Co_3O_4 can effectively accommodate the volume variations and improve the cycling stability of the hybrid network.[15-27] Finally, the *in situ* generated cobalt nanocrystals from Co_3O_4 might act as efficient catalyst to activate/promote the decomposition of Li_2O[15-27,34] and the reversible formation/decomposition of polymeric gel-like layer on anode surface,[32,33] leading to high reversible capacities of the In_2O_3–Co_3O_4 network.

In summary, we have rationally designed and synthesized a novel type of nanoporous In_2O_3–Co_3O_4 hybrid network *via* a facile freeze-drying and subsequent annealing approach using $InCl_3$–$K_3Co(CN)_6$ cyanogel as a precursor. When utilized as an anode in LIBs, the nanoporous In_2O_3–Co_3O_4 network manifests remarkable lithium-storage performance in terms of cycling stability and reversible capacity. For example, a high reversible capacity of 638.7 mA h g^{-1} can be delivered after 200 cycles at a current density of 100 mA g^{-1}. The synergistic effects between In_2O_3 and Co_3O_4 together with the nanoporous structure can be responsible for the remarkable capacity retention and high reversible capacities in the In_2O_3–Co_3O_4 network.

Experimental

Sample preparation

The $InCl_3$–$K_3Co(CN)_6$ cyanogel precursor was obtained by simply mixing freshly-made aqueous solutions of 0.6 M $InCl_3$ and 0.6 M $K_3Co(CN)_6$ with a volume ratio of 1:1 at room temperature. Subsequently, the $InCl_3$–$K_3Co(CN)_6$ cyanogel was freeze-dried and then the obtained xerogel was annealed at 600 ^oC in air for 3 h. The resulting black product was washed with distilled water and ethanol to remove KCl crystals and dried at 60 ^oC in air, yielding the nanoporous In_2O_3–Co_3O_4 hybrid network.

Characterization

The morphological, structural, and compositional features of the In_2O_3–Co_3O_4 network were characterized by X-ray powder diffraction (XRD, Rigaku D/max-RC), scanning electron microscopy (SEM, JEOL JSM 5610LV), and high-resolution transmission electron microscopy (HRTEM, JEOL JEM-2010F, 200 kV) equipped with an energy-dispersive X-ray spectrometer (EDS, Thermo Fisher Scientific). The Fourier transform infrared (FTIR) spectrum was recorded on a Bruker Tensor 27 spectrometer. Nitrogen adsorption/desorption test was performed using a Quantachrome Nova Station B instrument at 77 K.

Electrochemical measurements

Electrochemical measurements were carried out by 2025-type coin cells, which were assembled in an Ar-filled glove-box (Innovative Technology, IL-2GB). To prepare the anode, 70 wt% active material (In_2O_3–Co_3O_4 network), 15 wt% conductive carbon black (Super P), and 15 wt% binder (polyvinylidene fluoride, PVDF) were mixed in N-methyl-2-pyrrolidene (NMP) to form an uniform slurry, and then the slurry was coated on the surface of copper foams and dried under vacuum at 120 ^oC for 12 h. The counter electrode was lithium foil, and the electrolyte solution was 1 M $LiPF_6$ in ethylene carbonate (EC) and dimethyl carbonate (DMC) (1:1 v/v). Finally, the cells were aged for 12 h before tests. Charge–discharge characteristics were measured on a LANHE CT2001A battery tester (Wuhan LAND) in the potential range of 0.01-3.0 V at a current density of 100 mA g^{-1}.

Acknowledgments

The authors appreciate the financial supports from National Natural Science Foundation of China (51401110), Natural Science Foundation of Jiangsu Province (BK20130900), Natural Science Foundation of Jiangsu Higher Education Institutions of China (13KJB150026), National Undergraduate Training Programs for Innovation and Entrepreneurship, and a project funded by the Priority Academic Program Development of Jiangsu Higher Education Institutions.

Notes and references

Jiangsu Key Laboratory of New Power Batteries, Jiangsu Collaborative Innovation Center of Biomedical Functional Materials, School of Chemistry and Materials Science, Nanjing Normal University, Nanjing 210023, PR China. Fax: +86–25–85893286; Tel: +86–25–85891651;
E-mail: zjuwuping@njnu.edu.cn
§ Equal contribution to this work.

†Electronic Supplementary Information (ESI) available: [SEM images, nitrogen adsorption/desorption isotherms, microscopic structural characterization after cycling]. See DOI: 10.1039/c000000x/

1 J. Zai and X. Qian, *RSC Adv.*, 2015, **5**, 8814.
2 H. Geng, S. Li, Y. Pan, Y. Yang, J. Zheng and H. Gu, *RSC Adv.*, 2015, **5**, 52993.
3 H. Geng, D. Ge, S. Lu, J. Wang, Z. Ye, Y. Yang, J. Zheng and H. Gu, *Chem. Eur. J.*, 2015, **21**, 11129.
4 Y. Xiao, J. Zai, X. Li, Y. Gong, B. Li, Q. Han and X. Qian, *Nano Energy*, 2014, **6**, 51.
5 Y. Xiao, X. Li, J. Zai, K. Wang, Y. Gong, B. Li, Q. Han and X. Qian, *Nano-Micro Lett.*, 2014, **6**, 307.
6 Y. Xiao, J. Zai, L. Tao, B. Li, Q. Han, C. Yu and X. Qian, *Phys. Chem. Chem. Phys.*, 2013, 1**5**, 3939.
7 J. S. Chen and X. W. Lou, *Small*, 2013, **9**, 1877.
8 B. Li, J. Zai, Y. Xiao, Q. Han and X. Qian, *CrystEngComm*, 2014, **16**, 3318.
9 M. Dirican, M. Yanilmaz, K. Fu, Y. Lu, L. H. Kizil and X. Zhang, *J. Power Sources*, 2014, **264**, 240.
10 H. Jia, R. Kloepsch, X. He, J. P. Badillo, M. Winter and T. Placke, *J. Mater. Chem. A*, 2014, **2**, 17545.
11 X. Li, J. Liang, Z. Hou, Y. Zhu, Y. Wang and Y. Qian, *Chem. Commun.*, 2014, **50**, 13956.
12 H. Yang, T. Song, S. Lee, H. Han, F. Xia, A. Devadoss, W. Sigmund and U. Paik, *Electrochim. Acta*, 2013, **91**, 275.
13 D. Liu, W. Lei, S. Qin, L. Hou, Z. Liu, Q. Cui and Y. Chen, *J. Mater. Chem. A*, 2013, **1**, 5274.
14 S. Qin, W. Lei, D. Liu, P. Lamb and Y. Chen, *Mater. Lett.*, 2013, **91**, 5.
15 Q. Wang, J. Sun, Q. Wang, D. A. Zhang, L. Xing and X. Xue, *J. Mater. Chem. A*, 2015, **3**, 5083.
16 L. L. Xing, B. He, Y. X. Nie, P. Deng, C. X. Cui and X. Y. Xue, *Mater. Lett.*, 2013, **105**, 169.
17 W. Zhou, C. Cheng, J. Liu, Y. Y. Tay, J. Jiang, X. Jia, J. Zhang, H. Gong, H. H. Hng, T. Yu and H. J. Fan, *Adv. Funct. Mater.*, 2011, **21**, 2439.
18 W. Zhou, Y. Y. Tay, X. Jia, D. Y. Y. Wai, J. Jiang, H. H. Hoon and T. Yu, *Nanoscale*, 2012, **4**, 4459.
19 Y. Li, Y. Hu, H. Jiang, X. Hou and C. Li, *CrystEngComm*, 2013, **15**, 6715.
20 L. Zhang, H. B. Wu and X. W. Lou, *J. Am. Chem. Soc.*, 2013, **135**, 10664.
21 L. L. Xing, Y. Y. Zhao, J. Zhao, Y. X. Nie, P. Deng, Q. Wang and X. Y. Xue, *J. Alloys Compd.*, 2014, **586**, 28.
22 L. L. Xing, C. X. Cui, B. He, Y. X. Nie, P. Deng and X. Y. Xue, *Mater. Lett.*, 2013, **96**, 158.
23 C. Hua, X. Fang, Z. Wang and L. Chen, *Chem. Eur. J.*, 2014, **20**, 5487.
24 Q. Zhu, P. Wu, J. Zhang, W. Zhang, Y. Zhou, Y. Tang and T. Lu, *ChemSusChem*, 2015, **8**, 131.
25 X. Zhu, H. Shi, J. Yin, H. Zhu, Y. Zhou, Y. Tang, P. Wu and T. Lu, *RSC Adv.*, 2014, **4**, 34417.
26 X. Y. Xue, Z. H. Chen, L. L. Xing, S. Yuan and Y. J. Chen, *Chem. Commun.*, 2011, **47**, 5205.
27 X. Y. Xue, B. He, S. Yuan, L. L. Xing, Z. H. Chen and C. H. Ma, *Nanotechnology*, 2011, **22**, 395702.
28 J. Xu, X. Liu, Y. Chen, Y. Zhou, T. Lu and Y. Tang, *J. Mater. Chem.*, 2012, **22**, 23659.
29 M. Heibel, G. Kumar, C. Wyse, P. Bukovec and A. B. Bocarsly, *Chem. Mater.*, 1996, **8**, 1504.
30 J. Li, P. Wu, Y. Tang, X. Xu, Y. Zhou, Y. Chen and T. Lu, *CrystEngComm*, 2013, **15**, 10340.
31 K. Nakamoto, Infrared and Raman Spectra of Inorganic and Coordination Compounds, Part B: Applications in Coordination, Organometallic, and Bioinorganic Chemistry, Sixth Edition, Wiley, John Wiley & Sons, Inc., Hoboken (2009)
32 L. Su, Z. Zhou and P. Shen, *J. Phys. Chem. C*, 2012, **116**, 23974.
33 J. Yin, H. Shi, P. Wu, Q. Zhu, H. Wang, Y. Tang, Y. Zhou and T. Lu, *New J. Chem.*, 2014, **38**, 4036.
34 J. Zai, C. Yu, L. Tao, M. Xu, Y. Xiao, B. Li, Q. Han, K. Wang and X. Qian, *CrystEngComm*, 2013, 15, 6663.

Cyanogel-derived three-dimensional nanoporous In_2O_3–Co_3O_4 hybrid network as a high-capacity and long-life anode material for lithium-ion batteries